



SpecXMaster Technical Report

DP Technology *

March 25, 2026

 <https://specxmaster.bohrium.com>

Abstract

Intelligent spectroscopy serves as a pivotal element in AI-driven closed-loop scientific discovery, functioning as the critical bridge between matter structure and artificial intelligence. However, conventional expert-dependent spectral interpretation encounters substantial hurdles, including susceptibility to human bias and error, dependence on limited specialized expertise, and variability across interpreters. To address these challenges, we propose SpecXMaster, an intelligent framework leveraging Agentic Reinforcement Learning (RL) for NMR molecular spectral interpretation. SpecXMaster enables automated extraction of multiplicity information from both ^1H and ^{13}C spectra directly from raw FID (free induction decay) data. This end-to-end pipeline enables fully automated interpretation of NMR spectra into chemical structures. It demonstrates superior performance across multiple public NMR interpretation benchmarks and has been refined through iterative evaluations by professional chemical spectroscopists. We believe that SpecXMaster, as a novel methodological paradigm for spectral interpretation, will have a profound impact on the organic chemistry community.

1 Introduction

Nuclear Magnetic Resonance (NMR) spectroscopy stands as the cornerstone of structural chemistry, functioning as the primary analytical tool for the definitive identification and characterization of organic compounds. By providing an intricate map of molecular environments and connectivity, NMR spectra serve as the "molecular fingerprints" that enable researchers to validate synthetic outcomes and explore complex chemical spaces [1]. In the era of AI-driven closed-loop scientific discovery, the ability to rapidly and accurately interpret spectroscopic data has transitioned from a mere routine task to a critical bottleneck in the innovation pipeline [2]. The integration of high-throughput experimental platforms with automated data acquisition systems has generated vast amounts of raw Free Induction Decay (FID) data, necessitating a paradigm shift in how these signals are translated into chemical knowledge. Consequently, the development of robust, intelligent methodologies for structural elucidation is no longer merely a technical pursuit but a prerequisite for accelerating the pace of modern chemical research and bridging the gap between raw physical observations and actionable molecular insights.

Despite the analytical power of NMR spectroscopy, translating spectral data into definitive molecular structures remains an inherently expert-dependent process. This reliance on human intervention introduces critical hurdles that impede the scalability of modern chemical research. Manual interpretation, as a deductive process, is highly susceptible to human bias and error, heavily influenced by a researcher's prior expectations and subjective experience. Even for seasoned spectroscopists, navigating congested spectral regions or interpreting complex splitting patterns is prone to cognitive fatigue and oversight, potentially leading to misassignments that can derail downstream synthetic efforts. Furthermore, the steep learning curve required to master NMR interpretation creates an "expertise gap," where the availability of high-level expertise becomes the scarcest resource in a laboratory.

* Full authorship contribution statements appear at the end of the document.

As high-throughput synthesis and automated sampling become standard, the human interpreter has emerged as the primary bottleneck; data acquisition can take minutes, whereas rigorous elucidation may require hours or even days [3]. Compounding this issue is significant inter-interpreter variability, where the same set of ^1H and ^{13}C spectra can yield divergent structural hypotheses depending on an expert's individual heuristic approach, thereby complicating data reproducibility and the standardization of chemical databases. In summary, the conventional manual workflow is increasingly incompatible with the demands of AI-driven, autonomous discovery cycles. To bridge this gap, transitioning from "expert-assisted" to "machine-autonomous" spectral interpretation is not merely an optimization but a structural necessity for the future of organic chemistry.

Computational methods have fundamentally revolutionized NMR spectroscopy, driving significant advancements in structural biology and modern chemistry [4]. Quantum chemical (QM) methods provide precise predictions of NMR parameters for detailed characterization, while machine learning (ML) techniques complement these by automating spectral assignments and predicting chemical shifts. The rapid advent of "SpectraML" (Spectroscopy Machine Learning) has catalyzed a shift from traditional expert-dependent workflows toward automated analysis capable of handling high-dimensional data [5]. In forward tasks (molecule-to-spectrum prediction), frameworks such as NMRNet utilize SE(3) Transformers to model atomic environments [6]. Furthermore, semi-supervised approaches have been proposed that leverage millions of unlabeled spectra for training, addressing the scarcity of peak-assigned NMR datasets [7]. The field has increasingly focused on inverse tasks (spectrum-to-molecule inference), where multitask learning frameworks combining CNNs and Transformers can predict molecular connectivity directly from 1D spectra, significantly reducing the structural search space [8]. More recently, the emergence of multimodal Large Language Models (LLMs) such as SpectraLLM [9], MolSpectLLM [10], and Spectro [11] has enabled joint reasoning across multiple spectroscopic modalities, including NMR, IR, and MS, to mimic the holistic approach of human experts. Furthermore, frameworks like NMR-Solver [12] integrate spectral-guided fragment optimization to enable interpretable reasoning and efficient refinement of molecular candidates, while DeepSPInN formulates elucidation as a Markov decision process (MDP) solved via deep reinforcement learning [13]. While large-scale experimental databases like NMRexp now provide millions of records to train models [14], significant barriers to true automated intelligence persist.

Despite the rapid progress in computational spectroscopy, several critical gaps continue to hinder the practical deployment of AI in chemical research. Most existing frameworks suffer from an incomplete processing pipeline, frequently relying on simplified chemical shift lists or peak tables rather than directly interfacing with raw FID data, which remains a critical bottleneck for training truly robust and generalizable models. Furthermore, current methodologies often exhibit poor generalization when confronted with complex or novel molecules, frequently underperforming in real-world applications due to inherent algorithmic limitations and a heavy reliance on pre-existing structural databases or known structural information. Perhaps most significantly, these systems often lack the "intellectual" feedback and iterative reasoning capabilities of professional spectroscopists; they typically function as one-way mapping tools that neglect prior chemical knowledge and fail to perform the self-reflective logical deduction required to resolve discrepancies in experimental data.

To address these identified challenges, we propose SpecXMaster, an intelligent framework that introduces a novel methodological paradigm by leveraging Agentic RL for NMR spectral interpretation. Unlike traditional models that frequently rely on simplified chemical shift lists or peak tables, SpecXMaster employs an end-to-end pipeline that directly interfaces with raw FID data. By incorporating advanced signal processing techniques, the framework automates the extraction of quantitative peak parameters and multiplicity information from both NMR spectra of ^1H and ^{13}C .

As shown in **Figure 1**, SpecXMaster effectively translates complex physical signals into standardized, structured representations of NMR signals, which serve as the primary input for a Multi-step Agent that operates within a specialized tool environment featuring **Generate**, **Search**, **Repair**, and **Rerank** capabilities. By mimicking the iterative reasoning, discrepancy analysis, and error-correction logic of professional spectroscopists, SpecXMaster achieves an automated transition from raw NMR signals to precise chemical structures and comprehensive elucidation reports. This agentic approach moves beyond simple numerical error matching to assess overall structural plausibility, offering a robust, interpretable, and scalable solution for the organic chemistry community.

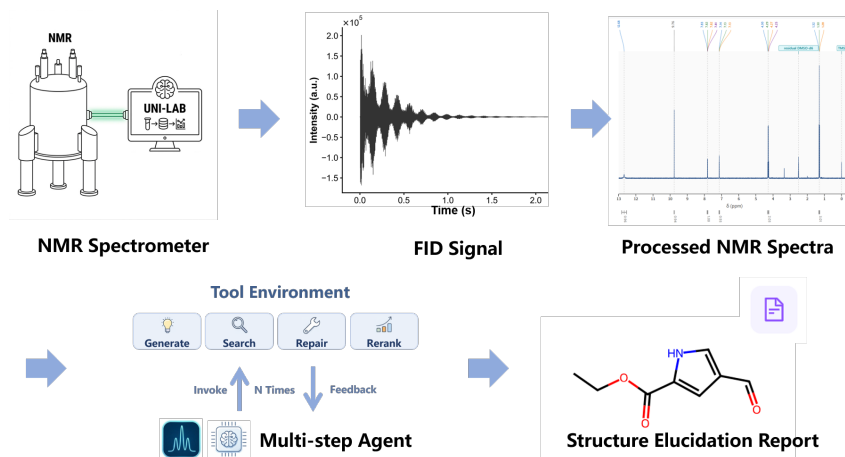


Figure 1: End-to-end pipeline of SpecXMaster

2 Full Processing Steps from FID to NMR Spectrum

2.1 Overview

NMR instruments record experimental signals in the form of **Free Induction Decay (FID)** time-domain data. Converting FID signals into interpretable spectra and structured chemical information is a critical step in automated NMR analysis.

We developed a **Python-based automated FID processing and spectral interpretation module** that transforms raw instrument output into:

- frequency-domain NMR spectra
- peak lists and multiplet annotations
- quantitative peak parameters
- structured textual representations of NMR signals

This module serves as the **front-end spectral processing component** of the multi-agent NMR analysis system, bridging raw experimental data and downstream structure interpretation modules.

The pipeline integrates conventional digital signal processing methods with machine learning-based multiplet identification to enable robust spectral analysis across diverse spectra.

2.2 System Architecture

The automated FID processing system consists of four major stages:

1. FID preprocessing
2. Fourier transformation and spectrum generation
3. Peak detection and multiplet identification
4. Spectral annotation and text generation

The system is implemented in Python using numerical computing libraries for spectral processing and neural network frameworks for multiplet classification.

2.3 Signal Transformation

The raw FID signal must first be transformed from the time domain into the frequency domain. This stage includes apodization, zero filling, and Fourier transformation. The raw FID data is read and processed using the nmrglue library [15].

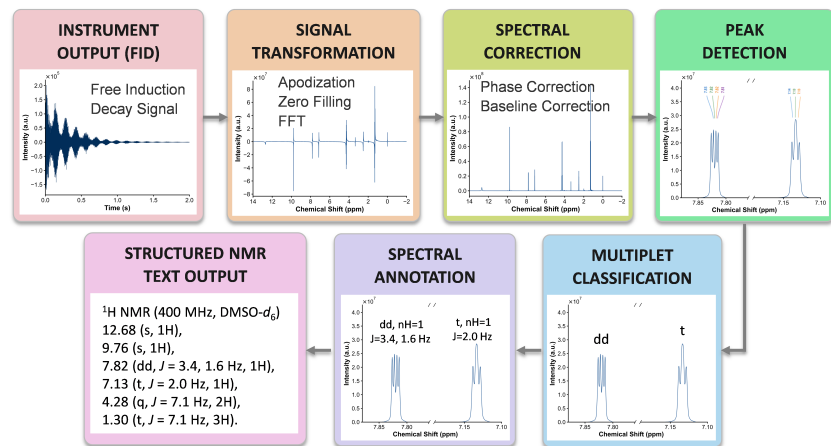


Figure 2: Overview of Nuclear Magnetic Resonance (NMR) Data Processing

Apodization: Apodization is applied to reduce truncation artifacts and improve the signal-to-noise ratio. The system supports several window functions commonly used in NMR signal processing [16], including exponential multiplication, Gaussian weighting and sine-bell apodization. These window functions can be parameterized to balance spectral resolution and sensitivity depending on experimental conditions.

Zero Filling: Zero filling is used to increase digital resolution in the frequency domain [17]. The original FID signal is extended by appending zeros until the signal length reaches a power-of-two value, which also improves the efficiency of the Fourier transform.

Fourier Transformation: After preprocessing, the time-domain FID signal $s(t)$ is converted into a frequency-domain spectrum using the Fast Fourier Transform (FFT) [18]:

$$S(\omega) = \mathcal{F}\{s(t)\} \quad (1)$$

where $S(\omega)$ represents the frequency-domain spectral intensity. The resulting spectrum represents resonance signals as peaks located at characteristic chemical shift positions.

2.4 Spectral Correction

Following Fourier transformation, the spectrum typically contains distortions introduced during acquisition and signal processing. These artifacts must be corrected before reliable peak detection can be performed.

Phase Correction: Phase distortions arise from imperfections in receiver timing and instrument electronics. If uncorrected, these distortions cause asymmetric or dispersive peak shapes. Automatic phase correction is implemented based on the ACME algorithm [19], which optimizes zero-order and first-order phase parameters based on entropy minimization. The optimization objective aims to minimize spectral asymmetry and maximize peak sharpness.

Baseline Correction: Baseline distortions may arise from instrument drift, solvent suppression artifacts, or truncation effects. Baseline correction is performed using the polynomial fitting and the improved asymmetric least squares (IASLS) algorithm combined with iterative masking of detected peaks using the pybaselines pack [20]. This procedure prevents the fitting process from being influenced by true resonance signals. After baseline correction, the spectrum exhibits a stable baseline suitable for quantitative peak analysis.

Peak Detection: Peak detection identifies candidate resonance signals from the processed spectrum [21]. The detection procedure consists of three main stages, including "noise level estimation", "local maxima detection" and "peak boundary determination". Noise levels are estimated from baseline regions of the spectrum. Peaks are identified based on signal-to-noise thresholds combined with local maximum detection. For each detected peak, the following parameters are extracted:

chemical shift (δ , ppm), peak intensity, peak width, and integrated peak area. Overlapping signals are segmented using derivative-based boundary detection.

2.5 Multiplet Identification and Spectral Annotation

After peak detection, clusters of neighboring peaks are analyzed to determine multiplet patterns arising from spin–spin coupling. Rule-based multiplet identification often fails when signals overlap or when spectra contain distortions, while machine learning can effectively solve this problem [22, 23]. To improve robustness, we implemented a **neural network-based multiplet classification model**. The model takes a localized spectral segment centered around candidate peaks as input and predicts the multiplet category. The supported multiplet types include: singlet(s), doublet(d), triplet(t), quartet(q), multiplet(dd, td, dt, ddd.....) and complex or overlapping patterns(m). The neural network was trained on a dataset of annotated spectra containing diverse multiplet patterns, which improves multiplet recognition accuracy, particularly in spectra containing partially overlapping signals.

Once peaks and multiplets are identified, the system generates annotated spectral information, including chemical shift values, multiplicity, integration values, and peak grouping information. Each detected signal is represented as a structured entry containing all extracted parameters.

2.6 Structured NMR Text Generation

To support downstream automated interpretation, spectral annotations are converted into standardized textual descriptions. A selected example output is illustrated:

1H NMR (400 MHz, CDCl₃): 7.26 (d, J = 8.4 Hz, 2H), 6.85 (d, J = 8.4 Hz, 2H), 3.78 (s, 3H)

This representation allows seamless integration with structure elucidation algorithms, chemical databases, and downstream reasoning modules.

3 Agent Architecture

3.1 Overview

Figure 3 illustrates the overall workflow of SpecXMaster, our agentic framework for NMR-based structure elucidation [24, 25]. Starting from the input NMR observation, the system first constructs a compact decision state that summarizes the current reasoning context, including the NMR summary, the current candidate pool, aggregated matching signals, and trajectory-level information such as history, budget, uncertainty, and diversity. Based on this state, the agent policy selects the next operation and, when necessary, produces the corresponding tool arguments, following the general paradigm of tool-augmented language models that learn to invoke external functions in a context-dependent manner [26, 27].

The available actions include candidate generation, candidate search, local repair, and reranking. After each action is executed, the environment returns structured feedback in the form of candidate updates, equivalence signals, and alignment signals. These feedback signals are then incorporated into the next-round state update, forming a closed-loop decision process. The interaction continues until the agent determines that the current candidate set is sufficiently good and outputs the final molecular structure.

Unlike one-shot structure prediction, SpecXMaster formulates NMR interpretation as an iterative reasoning-and-action process over a tool environment, where the model repeatedly evaluates the current state and determines the next step under intermediate feedback [27–29]. The key role of the agent is therefore not to generate the final molecule in a single step, but to adaptively decide how to explore, refine, and evaluate candidate structures under intermediate feedback.

3.2 Problem Formulation

Formally, given an observation x , the agent interacts with a tool environment \mathcal{T} for at most T rounds. At round t , the policy produces a state-conditioned action

$$a_t \sim \pi_\theta(\cdot | s_t), \quad (2)$$

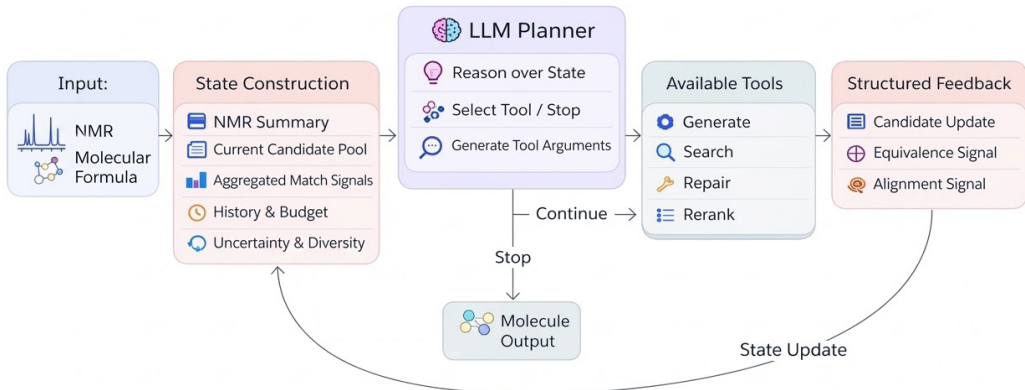


Figure 3: Overview of SpecXMaster, the proposed agentic framework for NMR-based molecular structure elucidation. The agent iteratively constructs a decision state, selects actions over the tool environment, receives structured feedback, and updates the state until termination.

where s_t denotes the current reasoning state and π_θ denotes the agent policy.

Each action is factorized as

$$a_t = (a_t^{\text{type}}, a_t^{\text{arg}}), \quad (3)$$

where a_t^{type} specifies the molecular operation to invoke and a_t^{arg} specifies its corresponding arguments. In the current system,

$$a_t^{\text{type}} \in \{\text{Generate}, \text{Search}, \text{Optimize}, \text{ReRank}, \text{Stop}\}. \quad (4)$$

After executing a_t , the tool environment returns a structured observation

$$o_t = \mathcal{T}(a_t), \quad (5)$$

and the next reasoning state is updated as

$$s_{t+1} = g(s_t, a_t, o_t), \quad (6)$$

where g is the state update operator.

The full reasoning trajectory is therefore

$$\tau = (x, s_1, a_1, o_1, s_2, a_2, o_2, \dots, s_T, a_T, o_T). \quad (7)$$

At termination, the system outputs the final molecular hypothesis

$$\hat{y} = \phi(C_T), \quad (8)$$

where C_T denotes the terminal candidate pool and $\phi(\cdot)$ denotes the final selection rule.

3.3 Tool Environment

We define a unified tool environment \mathcal{T} that exposes a small set of molecular operations to the agent. In the current framework, these operations include candidate generation, candidate search, local optimization, and final re-ranking. Rather than treating these tools as isolated modules, we regard them as the external action interface through which the agent explores and refines molecular hypotheses.

Generate. The *Generate* tool employs an autoregressive model to generate end-to-end molecular structure from spectral inputs, inspired by the approach of NMRPeak [30]. Concretely, the model predicts molecular SMILES sequences conditioned on the given NMR spectra. To obtain a diverse yet high-quality hypothesis set, beam search decoding is adopted to produce a ranked collection of candidate molecules.

This generation stage provides the agent with an initial pool of chemically valid structures that are broadly consistent with the observed spectral patterns. The resulting candidate set serves as the starting point for subsequent tool interactions, including candidate search, local refinement, and final re-ranking, thereby enabling efficient exploration of the molecular hypothesis space.

Database search. The *Search* tool enables rapid retrieval of spectrally similar molecules from a large-scale repository of known compounds. It leverages the database introduced in NMR-Solver [12], which contains 106 million chemically valid molecules curated from the PubChem [31] dataset. Each entry is associated with simulated ^1H and ^{13}C NMR spectra, providing a comprehensive reference space for efficient spectrum-based matching. Given an input NMR spectrum, the tool returns a ranked list of candidate molecular structures whose simulated spectra are most consistent with the query.

To achieve both efficiency and retrieval quality, the search is performed in two stages: an initial retrieval using vector representations with an HNSW [32] index identifies candidate molecules, followed by re-ranking based on peak-level set similarity of the spectra. This hybrid strategy enables sub-second querying at the scale of hundreds of millions of compounds while maintaining high matching fidelity.

Repair. The *Repair* tool is implemented on top of REINVENT4 [33] and is used for targeted optimization of candidate molecules during the iterative reasoning process. Given an input candidate molecule m , the tool performs reinforcement-learning-based molecular optimization to improve its consistency with the observed spectrum, rather than generating a new structure from scratch, following the general paradigm of goal-directed molecular optimization from a starting compound [34, 35].

Concretely, the repair objective is defined through a forward spectral prediction module developed in-house. Given a molecule m , the predictor produces its simulated spectrum $\hat{s}(m)$, which is then compared against the observed spectrum s^* through a similarity function $\text{Sim}(\hat{s}(m), s^*)$. This similarity score is used as the reward signal:

$$R_{\text{repair}}(m) = \text{Sim}(\hat{s}(m), s^*). \quad (9)$$

Starting from the current candidate, REINVENT4 optimizes the molecular policy toward candidates with higher spectral reward. The resulting tool is therefore particularly useful in cases where the current candidate pool already contains structurally plausible molecules, but additional local optimization is needed to improve spectrum-level agreement, consistent with prior work on constrained or starting-point-guided molecular optimization [34, 36].

Peak assignment. This *Assign* tool addresses the problem of NMR peak assignment. Given a molecular structure and an experimental spectrum, the objective is to establish a correspondence between experimental signals and structurally defined sites. This is formulated as a structured relation $A \subseteq \mathcal{I} \times \mathcal{J}$, where \mathcal{I} denotes the set of structural sites and \mathcal{J} denotes the set of observed spectral signals. The feasible assignment space is constrained by structural and observational consistency requirements $A \in \mathcal{A}$.

In practice, the set of structural sites \mathcal{I} is constructed through an equivalence analysis that groups atoms indistinguishable under symmetry or dynamic averaging. Since NMR experiments probe ensemble-averaged signals, assignment is performed at the level of equivalence groups rather than individual atoms.

The assignment is constructed based on multiple complementary sources of compatibility. For each potential pair (i, j) between a structural site and an experimental signal, a compatibility function $\phi(i, j)$ is defined to characterize their agreement:

$$\phi(i, j) = \phi_{\delta}(i, j) \cdot \phi_{\text{disc}}(i, j) \cdot \phi_J(i, j). \quad (10)$$

Here, ϕ_{δ} measures the agreement between predicted and observed chemical shifts based on structure-derived shift estimates, ϕ_{disc} encodes compatibility between discrete structural motifs and observed multiplicity patterns, and ϕ_J captures relational consistency arising from predicted scalar coupling relationships. These components are constructed from empirical rules and physically motivated relationships and are interpreted as compatibility measures rather than exact predictions.

Chemical shifts are predicted using a structure-based deep learning model, trained on over a million reference spectra, providing expected reference values for each site [7]. Coupling values are estimated by Karplus-type relations [37] of the form

$$J(\theta) = A \cos^2 \theta + B \cos \theta + C, \quad (11)$$

where θ denotes the dihedral angle along the coupling pathway. These relations provide a physically grounded connection between molecular structure and observable coupling patterns, incorporating both empirical rules and geometric priors.

In addition, the assignment process explicitly accounts for non-ideal experimental conditions. The observed spectrum can be viewed as a partially observed realization of the underlying structural response:

$$X = g(c, A) + \varepsilon, \quad (12)$$

where g denotes the structural mapping to observable signals and ε captures effects such as missing, merged, or weakly resolved signals. As a result, compatibility is evaluated in a tolerant manner, allowing deviations consistent with realistic measurement conditions.

Overall, peak assignment is formulated as a structured correspondence problem that integrates empirical knowledge, physical relations, and observational constraints to produce a globally consistent mapping between structural sites and experimental signals.

Candidate rerank. The *Rerank* tool extends the peak assignment framework from a single structure to a candidate set. For each candidate structure $c \in \mathcal{C}$, a peak assignment procedure is first performed to establish a mapping between structural sites and experimental signals. Rather than comparing structures directly, candidates are evaluated based on the quality of their best achievable spectral explanation.

Formally, the score of a candidate structure is defined as the minimum assignment cost over all feasible assignment configurations:

$$S(c) = \min_{A \in \mathcal{A}(c)} \mathcal{L}(A | c, X), \quad (13)$$

where X denotes the experimental spectrum, A represents a valid assignment configuration, and $\mathcal{A}(c)$ is the set of all feasible assignments under structural and observational constraints.

The total cost function is composed of multiple components capturing different aspects of assignment quality:

$$\mathcal{L}(A | c, X) = \lambda_{\text{match}} \mathcal{L}_{\text{match}} + \lambda_{\text{cov}} \mathcal{L}_{\text{coverage}} + \lambda_{\text{obs}} \mathcal{L}_{\text{observation}}. \quad (14)$$

The matching term $\mathcal{L}_{\text{match}}$ measures local agreement between assigned pairs of structural sites and experimental signals:

$$\mathcal{L}_{\text{match}} = \sum_{(i,j) \in A} \ell(i, j),$$

where $\ell(i, j)$ encodes deviations in continuous attributes and inconsistencies in discrete structural patterns. The coverage term penalizes incomplete explanations of the spectrum:

$$\mathcal{L}_{\text{coverage}} = \alpha N_{\text{unassigned sites}} + \beta N_{\text{unexplained signals}}. \quad (15)$$

In addition, an observation term $\mathcal{L}_{\text{observation}}$ accounts for non-ideal experimental effects through controlled tolerance of missing, merged, or weakly resolved signals.

Importantly, the assignment A is obtained under global consistency constraints, so that the optimization is not a sum of independent local matches but a structured matching problem over the entire spectrum. The resulting score therefore reflects the best self-consistent explanation of the observed data by a given candidate.

The final prediction is obtained by selecting the candidate with the lowest assignment cost:

$$c^* = \arg \min_{c \in \mathcal{C}} S(c). \quad (16)$$

Hard-case processor. As part of the *ReRank* module, we introduce a hard-case processor based on hyperbolic representation learning to improve discrimination on challenging near-tie candidates. This design is inspired by prior work on hyperbolic representation learning, which has shown that hyperbolic geometry is particularly effective for modeling hierarchical or fine-grained relational structure in representation space [38–40]. It is also motivated by recent findings that hyperbolic scoring can improve difficult ranking problems with small margins between highly similar candidates [41]. The key idea is that hyperbolic geometry provides larger effective separation in crowded local neighborhoods, making it more suitable for distinguishing small-margin candidates than conventional Euclidean similarity.

Let $\mathbf{z}^{(s)} \in \mathbb{R}^d$ denote the projected spectrum representation and $\mathbf{z}_i^{(m)} \in \mathbb{R}^d$ denote the projected representation of the i -th candidate molecule after integrating molecular and prior information. We

use Uni-Mol [42] for molecular representations and BART [43] for spectral representations, followed by NMRPeak. We map these Euclidean vectors into the Lorentz model of hyperbolic space,

$$\mathbb{H}_\kappa^d = \{ \mathbf{x} \in \mathbb{R}^{d+1} \mid \langle \mathbf{x}, \mathbf{x} \rangle_{\mathcal{L}} = -\kappa, x_0 > 0 \}, \quad (17)$$

where $\kappa > 0$ is the curvature radius and $\langle \cdot, \cdot \rangle_{\mathcal{L}}$ is the Lorentz inner product

$$\langle \mathbf{x}, \mathbf{y} \rangle_{\mathcal{L}} = -x_0 y_0 + \sum_{j=1}^d x_j y_j. \quad (18)$$

We first obtain normalized Euclidean projections

$$\tilde{\mathbf{z}}^{(s)} = \text{LN}(\mathbf{z}^{(s)}), \quad \tilde{\mathbf{z}}_i^{(m)} = \text{LN}(\mathbf{z}_i^{(m)}), \quad (19)$$

and then lift them to hyperbolic points using the exponential map at the origin:

$$\mathbf{h}^{(s)} = \exp_{\mathbf{o}}^\kappa(\tilde{\mathbf{z}}^{(s)}), \quad \mathbf{h}_i^{(m)} = \exp_{\mathbf{o}}^\kappa(\tilde{\mathbf{z}}_i^{(m)}), \quad (20)$$

where $\mathbf{o} = (\sqrt{\kappa}, 0, \dots, 0)$ is the hyperbolic origin. The hyperbolic geodesic distance between the spectrum and the i -th candidate is then

$$d_{\mathbb{H}}(\mathbf{h}^{(s)}, \mathbf{h}_i^{(m)}) = \sqrt{\kappa} \operatorname{arcosh} \left(-\frac{\langle \mathbf{h}^{(s)}, \mathbf{h}_i^{(m)} \rangle_{\mathcal{L}}}{\kappa} \right). \quad (21)$$

We define the hard-case score using the negative geodesic distance

$$s_i^{\text{hard}} = -d_{\mathbb{H}}(\mathbf{h}^{(s)}, \mathbf{h}_i^{(m)}), \quad (22)$$

so that candidates more consistent with the spectrum receive larger scores.

To further emphasize hard-case discrimination, we optimize the processor with a hybrid objective that combines hyperbolic contrastive learning and margin-based hard-negative ranking:

$$\mathcal{L}_{\text{hard}} = \mathcal{L}_{\text{con}} + \lambda_{\text{rank}} \mathcal{L}_{\text{rank}} + \lambda_{\text{reg}} \mathcal{L}_{\text{reg}}, \quad (23)$$

where λ_{rank} and λ_{reg} balance the contributions of the auxiliary objectives.

The contrastive term is defined as

$$\mathcal{L}_{\text{con}} = -\log \frac{\exp(s_{i^+}^{\text{hard}}/\eta)}{\exp(s_{i^+}^{\text{hard}}/\eta) + \sum_{i^- \in \mathcal{N}_{\text{hard}}} \exp(s_{i^-}^{\text{hard}}/\eta)}, \quad (24)$$

where $\eta > 0$ is a temperature parameter and $\mathcal{N}_{\text{hard}}$ denotes the mined hard-negative set.

To further enlarge the separation margin between the positive candidate and hard negatives, we introduce a ranking term

$$\mathcal{L}_{\text{rank}} = \sum_{i^- \in \mathcal{N}_{\text{hard}}} [m - s_{i^+}^{\text{hard}} + s_{i^-}^{\text{hard}}]_+, \quad (25)$$

where $m > 0$ is a ranking margin and $[\cdot]_+ = \max(\cdot, 0)$.

Finally, to stabilize the learned representation space, we use a regularization term

$$\mathcal{L}_{\text{reg}} = \left\| \tilde{\mathbf{z}}^{(s)} \right\|_2^2 + \left\| \tilde{\mathbf{z}}_{i^+}^{(m)} \right\|_2^2 + \sum_{i^- \in \mathcal{N}_{\text{hard}}} \left\| \tilde{\mathbf{z}}_{i^-}^{(m)} \right\|_2^2. \quad (26)$$

This objective simultaneously improves global separability, enforces a larger margin on hard negatives, and stabilizes the local geometry of the learned embedding space. The resulting hard-case score is then used as a dedicated signal for difficult candidates before downstream ranking.

3.4 State Representation and Structured Feedback

The agent operates on a compact state representation that summarizes the current progress of the reasoning trajectory. Rather than reprocessing raw spectral signals at every round, the policy reasons over a state s_t that captures both the current hypothesis set and the interaction context. Specifically, at round t , the state contains the current candidate pool C_t , candidate-level summary signals, equivalence-related judgments over the current hypotheses, as well as the action history and the remaining interaction budget.

After executing an action a_t , the tool environment returns a structured observation rather than raw tool outputs. We use a compact feedback interface so that the policy can reason over high-level progress signals instead of low-level execution details. In the current framework, the observation is summarized as

$$o_t = (c_t, e_t, m_t), \quad (27)$$

where c_t denotes the **candidate summary**, e_t denotes the **equivalence judgment**, and m_t denotes the **alignment information**. Here, c_t summarizes the updated status of the candidate pool, e_t indicates whether multiple candidates correspond to equivalent or near-equivalent structural hypotheses, and m_t reflects how well the current hypothesis set agrees with the spectral and chemistry-aware evaluation signals.

4 Agentic Reinforcement Learning Framework

4.1 Policy Formulation

Based on the interaction process defined in Eqs. (2)–(8), we model the agent as a state-conditioned stochastic policy over the tool environment [44]. Using the action factorization in Eq. (3), the policy is written as

$$\pi_\theta(a_t | s_t) = \pi_\theta(a_t^{\text{type}}, a_t^{\text{arg}} | s_t), \quad (28)$$

where s_t denotes the current reasoning state and a_t denotes the next molecular action.

The policy backbone is implemented by an LLM, which serves as a structured controller that selects molecular operations and instantiates their arguments, rather than acting as a generic free-form text generator [26, 45, 46]. At each round, it is responsible for selecting which molecular operation to invoke next, producing the corresponding arguments when needed, and determining whether the current reasoning process should terminate.

The policy is optimized by maximizing the expected return of the full reasoning process:

$$\max_{\theta} \mathbb{E}_{\tau \sim \pi_\theta} \left[\sum_{t=1}^T r_t \right], \quad (29)$$

where r_t is the step-level reward assigned after executing action a_t and observing feedback o_t .

This formulation is suitable for NMR-based structure elucidation because the usefulness of an action is often delayed and depends on subsequent refinement steps.

4.2 Reward Design

Given the reasoning trajectory in Eq. (7), we assign a step-level reward after each action–observation pair (a_t, o_t) . The reward at step t is defined as

$$r_t = \lambda_{\text{fmt}} r_t^{\text{fmt}} + \lambda_{\text{eff}} r_t^{\text{eff}} + \lambda_{\text{tool}} r_t^{\text{tool}} + \lambda_{\text{align}} r_t^{\text{align}}, \quad (30)$$

where each term captures one aspect of desirable agent behavior.

Format reward. Let \mathcal{V}_{fmt} denote the set of valid and executable action outputs. We define

$$r_t^{\text{fmt}} = \mathbf{1}[a_t \in \mathcal{V}_{\text{fmt}}]. \quad (31)$$

Efficiency reward. Let T_0 denote a target reasoning budget. We define

$$r_t^{\text{eff}} = -\mathbf{1}[t > T_0]. \quad (32)$$

Tool-usage reward. Let $\mathcal{V}_{\text{tool}}$ denote the set of successful tool invocations, $\mathcal{P}_{\text{tool}}$ denote the set of productive tool outcomes, and $\mathcal{F}_{\text{tool}}$ denote the set of failed or invalid tool calls. The tool-usage reward is defined as

$$r_t^{\text{tool}} = \alpha_{\text{succ}} \mathbf{1}[(a_t, o_t) \in \mathcal{V}_{\text{tool}}] + \alpha_{\text{prog}} \mathbf{1}[(a_t, o_t) \in \mathcal{P}_{\text{tool}}] - \alpha_{\text{fail}} \mathbf{1}[(a_t, o_t) \in \mathcal{F}_{\text{tool}}], \quad (33)$$

where $\alpha_{\text{succ}}, \alpha_{\text{prog}}, \alpha_{\text{fail}} > 0$ are tunable coefficients.

Alignment reward. Given the structured feedback in Eq. (27), let $r_{\text{cand}}(o_t)$ measure improvement in candidate summary and let $r_{\text{eq}}(o_t)$ measure reduction of redundant or unstable hypotheses. We define

$$r_t^{\text{align}} = \beta_1 r_{\text{cand}}(o_t) + \beta_2 r_{\text{eq}}(o_t), \quad (34)$$

where $\beta_1, \beta_2 \geq 0$ are weighting coefficients.

Accordingly, the total return of a reasoning process is defined as the sum of step-level rewards along the trajectory:

$$R(\tau) = \sum_{t=1}^T r_t. \quad (35)$$

4.3 Training Strategy

We adopt a two-stage training strategy. In the first stage, the policy is initialized with supervised fine-tuning (SFT) or behavior-cloned warm-start data so that the model can learn the required action format and interact with the tool environment in a stable and executable manner. In the second stage, we further optimize the initialized policy using Group Relative Policy Optimization (GRPO) [47–49].

For each training instance, we sample a group of responses

$$\{y_i\}_{i=1}^G, \quad y_i \sim \pi_{\theta_{\text{old}}}(\cdot | x), \quad (36)$$

where each response y_i corresponds to one complete rollout under the current policy and therefore induces a full reasoning process τ_i . For each sampled response, we execute the corresponding multi-step interaction in the tool environment and compute its total return

$$R_i = R(\tau_i) = \sum_{t=1}^{T_i} r_{i,t}. \quad (37)$$

Following the group-relative formulation, we normalize rewards within each sampled group to obtain the relative advantage:

$$\hat{A}_i = \frac{R_i - \mu_R}{\sigma_R + \epsilon}, \quad \mu_R = \frac{1}{G} \sum_{j=1}^G R_j, \quad \sigma_R = \sqrt{\frac{1}{G} \sum_{j=1}^G (R_j - \mu_R)^2}. \quad (38)$$

Here, ϵ is a small constant for numerical stability.

Let $y_{i,t}$ denote the t -th optimized token in response y_i . Define the policy ratio

$$\rho_{i,t}(\theta) = \frac{\pi_{\theta}(y_{i,t} | x, y_{i,<t})}{\pi_{\theta_{\text{old}}}(y_{i,t} | x, y_{i,<t})}. \quad (39)$$

Then the GRPO objective is

$$\mathcal{L}_{\text{GRPO}}(\theta) = -\frac{1}{G} \sum_{i=1}^G \frac{1}{|y_i|} \sum_{t=1}^{|y_i|} \min\left(\rho_{i,t}(\theta) \hat{A}_i, \text{clip}(\rho_{i,t}(\theta), 1 - \epsilon_c, 1 + \epsilon_c) \hat{A}_i\right), \quad (40)$$

where ϵ_c is the clipping coefficient.

5 Experiment

5.1 Experimental Setup

Baselines and compared methods. We compare SpecXMaster against three categories of methods. The first category is the standalone generation tool, which corresponds to the *Generate* module in our tool environment (Section 3.3). In this setting, molecular structures are predicted directly from spectral inputs without iterative multi-step decision making, and the resulting candidate list is used as a generation-based baseline.

The second category consists of workflow baselines. These baselines preserve the same overall tool environment, prompt format, and multi-step interaction protocol as SpecXMaster, but replace the trained agent policy with a general-purpose foundation model. In our experiments, we instantiate two workflow baselines using GPT-5.2 [50] and Qwen2.5-7B [51], respectively. This comparison is intended to isolate the value of the learned agent policy from the value of the tool environment itself.

The final category is the proposed SpecXMaster model. It is built on the same Qwen2.5-7B backbone as the corresponding workflow baseline, but uses a trained agent policy optimized through supervised fine-tuning and reinforcement learning (Section 4). Unless otherwise specified, all compared methods are evaluated under the same benchmark setting and input modes.

Benchmark setup, data split, and training data construction. We follow the benchmark construction and data split settings of NMRexp dataset [14] described in Xu et al. [30] to ensure fair and direct comparison with prior work. The overall statistics of the NMRexp dataset across different splits are summarized in Table 1. The dataset is divided into training, validation, and test sets, each containing spectrum–structure pairs.

Table 1: Statistics of the NMRexp dataset across different splits and spectrum types.

Split	Total	¹³ C spectra	¹ H spectra	Joint (¹³ C & ¹ H)
Train	920,796	786,240	805,224	670,668
Validation	48,463	41,383	42,366	35,286
Test	107,696	91,830	94,163	78,297
Overall	1,076,955	919,453	941,753	784,251

Training protocol. We adopt a two-stage training strategy, following the common practice of first performing supervised fine-tuning (SFT) to establish the desired output format and basic behavior, and then further improving the policy with reinforcement learning [52]. Since the generation tool has already been trained on the original training split, all agent-training data are constructed from the validation split of NMRexp, while the test split is reserved exclusively for evaluation. In the first stage, we perform SFT on 2,000 samples drawn from the validation split to teach the model the required structured output format and basic tool-use behavior. The SFT set consists of 1,000 Joint samples, 500 ¹³C spectra samples, and 500 ¹H spectra samples. In the second stage, starting from the SFT-initialized checkpoint, we perform online reinforcement learning on the full validation split. This design avoids overlap with the generator’s original training data and ensures that the agent is optimized on a split whose candidate structures are more consistent with the data distribution encountered during agent training.

Optimization details. For RL training, we use a batch size of 32 and train for 900 optimization steps. Unless otherwise specified, the same backbone model, tool environment, and evaluation protocol are used across all agent variants.

Evaluation metrics. Model performance is evaluated using the hit@*k* metric. For each query sample *i*, the model generates a ranked list of candidate molecules, and hit@*k* measures whether the ground-truth molecule appears within the top-*k* positions. Formally, hit@*k* is computed as

Method	hit@1			hit@3			hit@5		
	Joint	¹³ C spectra	¹ H spectra	Joint	¹³ C spectra	¹ H spectra	Joint	¹³ C spectra	¹ H spectra
Generation Tool	0.639	0.424	0.438	0.787	0.573	0.592	0.820	0.617	0.640
Workflow (GPT-5.2)	0.586	0.371	0.385	0.703	0.489	0.508	0.728	0.525	0.548
Workflow (Qwen2.5-7B)	0.563	0.348	0.362	0.678	0.464	0.483	0.701	0.498	0.521
SpecXMaster	0.702	0.455	0.450	0.822	0.590	0.589	0.840	0.625	0.629

Table 2: Main benchmark. We report hit@1, hit@3, and hit@5 under three input modes: Joint (¹³C & ¹H), ¹³C spectra, and ¹H spectra. The best result in each column is highlighted in bold.

$$\text{hit}@k = \frac{1}{N} \sum_{i=1}^N \mathbf{1}(\text{rank}_i \leq k), \quad (41)$$

where N denotes the total number of test samples, rank_i is the ranking position of the correct molecule for sample i , and $\mathbf{1}(\cdot)$ is the indicator function.

5.2 Main Benchmark Results

We first compare SpecXMaster against the standalone Generation Tool and two workflow baselines on the main benchmark. Following the current evaluation protocol, we report hit@1, hit@3, and hit@5 under three spectrum settings: Joint, ¹³C spectra, and ¹H spectra. The results are summarized in Table 2.

The most important observation is that SpecXMaster consistently achieves the strongest top-ranked performance among all compared systems. In particular, on hit@1, SpecXMaster reaches 0.702 on Joint, 0.455 on ¹³C spectra, and 0.450 on ¹H spectra, outperforming both workflow baselines by clear margins across all three spectrum settings. This result indicates that the advantage of SpecXMaster does not come simply from access to the same tool environment, but from a policy that is explicitly trained for NMR-guided multi-step decision making. In other words, the learned agent is better at deciding when to generate, when to search, when to repair, and how to rerank candidate structures based on intermediate feedback.

A second notable result is that the workflow baselines not only remain weaker than SpecXMaster, but also consistently underperform the standalone Generation Tool. This suggests that directly plugging a general-purpose LLM into the tool environment is not sufficient for this task. Although models such as GPT-5.2 and Qwen2.5-7B are strong general-purpose reasoners, they do not natively possess the domain-aligned inductive bias required for NMR interpretation, nor do they directly model the statistical regularities of spectrum-to-structure mapping. As a result, when used in a fixed prompting-based workflow, the additional decision layer may introduce extra noise instead of improving the candidate set. By contrast, the standalone Generation Tool is trained specifically for spectrum-conditioned molecular generation and therefore provides stronger direct spectral grounding even without iterative agent control.

At the same time, SpecXMaster improves over the Generation Tool on early precision across all three spectrum settings. On hit@1, the agent raises performance from 0.639 to 0.702 on Joint, from 0.424 to 0.455 on ¹³C spectra, and from 0.438 to 0.450 on ¹H spectra. On ¹³C spectra, the improvement also extends to hit@3 and hit@5, increasing from 0.573 to 0.590 and from 0.617 to 0.625, respectively. On ¹H spectra, SpecXMaster still achieves the best hit@1, while the standalone Generation Tool remains slightly stronger at hit@3 and hit@5, consistent with the original single-modality trend. Overall, these results show that SpecXMaster effectively combines spectrum-grounded generation with learned multi-step decision making, leading to the strongest overall top-ranked performance among the compared systems.

5.2.1 Effect of RL-based Agent Optimization

We evaluate the contribution of reinforcement learning by comparing three agent variants under the same tool environment: a fixed workflow baseline implemented with GPT-5.2, an SFT-only agent, and the final RL-optimized agent.

Method	hit@1			Format Validity			Case judgement		
	Joint	¹³ C spectra	¹ H spectra	Joint	¹³ C spectra	¹ H spectra	Joint	¹³ C spectra	¹ H spectra
Workflow (GPT-5.2)	0.586	0.371	0.385	0.744	0.648	0.676	0.301	0.689	0.781
SpecXMaster (SFT)	0.601	0.394	0.423	0.768	0.673	0.700	0.316	0.710	0.802
SpecXMaster (RL)	0.702	0.455	0.449	0.999	1.000	0.999	0.890	0.854	0.918

Table 3: Comparison between the fixed workflow baseline, the SFT-only agent, and the RL-optimized agent. The best result in each column is highlighted in bold.

Variant	hit@1			Avg. # steps			Useful action rate		
	Joint	¹³ C spectra	¹ H spectra	Joint	¹³ C spectra	¹ H spectra	Joint	¹³ C spectra	¹ H spectra
Full reward	0.702	0.455	0.449	4.18	4.96	4.71	0.352	0.331	0.339
w/o efficiency reward	0.699	0.452	0.445	5.34	6.52	6.08	0.309	0.286	0.293
w/o tool-usage reward	0.697	0.446	0.444	4.33	5.05	4.80	0.288	0.272	0.279
w/o alignment reward	0.691	0.443	0.438	4.15	4.88	4.62	0.356	0.335	0.342

Table 4: Reward ablation results. We report hit@1, average number of reasoning steps, and useful action rate under three spectrum settings.

Table 3 shows that reinforcement learning substantially improves the agent beyond the SFT-only initialization. In terms of final structure prediction, SpecXMaster (RL) consistently outperforms SpecXMaster (SFT) across all three spectrum settings. In particular, the hit@1 score improves from 0.601 to 0.702 on Joint, from 0.394 to 0.455 on ¹³C spectra, and from 0.423 to 0.449 on ¹H spectra. These results show that RL brings consistent gains over the SFT initialization across all three settings.

RL also brings a dramatic improvement in Format Validity. While the SFT policy already produces valid outputs in a substantial portion of cases, the RL-optimized policy pushes this metric to nearly perfect levels in all three settings (0.999/1.000/0.999 for Joint / ¹³C spectra / ¹H spectra). This indicates that RL does not merely improve ranking quality, but also stabilizes the interaction behavior of the agent, making its tool calls and stopping decisions much more reliable.

Most importantly, the improvement in Case judgement shows that RL changes the agent’s decision strategy rather than only refining surface-level output quality. Compared with the SFT policy, the RL policy achieves much higher case-judgement accuracy in every setting, with especially large gains on Joint (0.316 → 0.890) and ¹H spectra (0.802 → 0.918). This suggests that the RL-trained agent is substantially better at recognizing whether the current candidate pool is already good enough to stop or whether further optimization is needed. In other words, the main contribution of RL is not simply better generation, but better sequential decision making over the tool environment.

Finally, the workflow baseline remains below the learned agent in both final accuracy and decision-related metrics. This gap indicates that the observed gains do not come merely from having access to the same tools, but from learning how to use them adaptively through RL.

5.2.2 Reward Ablation

We next analyze the contribution of the step-level reward design by removing one reward component at a time, while keeping the extraction module and the default format reward enabled in all settings. The results in Table 4 show that the full reward delivers the best overall trade-off between final prediction quality, reasoning efficiency, and action quality.

Efficiency reward. When the efficiency reward is omitted, the average number of reasoning steps increases substantially across all three spectrum settings, confirming that this term is the primary mechanism for controlling trajectory length. Meanwhile, the accompanying decline in useful action rate indicates that many of the extra steps are unproductive, reflecting redundant exploration rather than effective progress.

Tool-usage reward. Without the tool-usage reward, the useful action rate drops consistently, together with a slight degradation in hit@1. This suggests that the tool-usage reward helps the policy

learn when invoking a tool is genuinely beneficial, rather than merely encouraging more frequent interactions with the tool environment.

Alignment reward. Ablating the alignment reward yields the largest reduction in hit@1 across all three spectrum settings, even though the average number of reasoning steps becomes slightly smaller and the useful action rate remains competitive. This suggests that the alignment reward is the most critical component for improving final prediction quality, as it directly encourages the policy to steer the candidate pool toward better spectral consistency.

6 Case Study

To demonstrate the practical utility and robustness of the SpecXMaster framework, we conducted a comprehensive case study on **Ethyl 4-formyl-1H-pyrrole-2-carboxylate**, a representative heterocyclic compound in synthetic organic chemistry. This case study illustrates the seamless transition from raw physical signals to a refined chemical structure. (Figure 4)

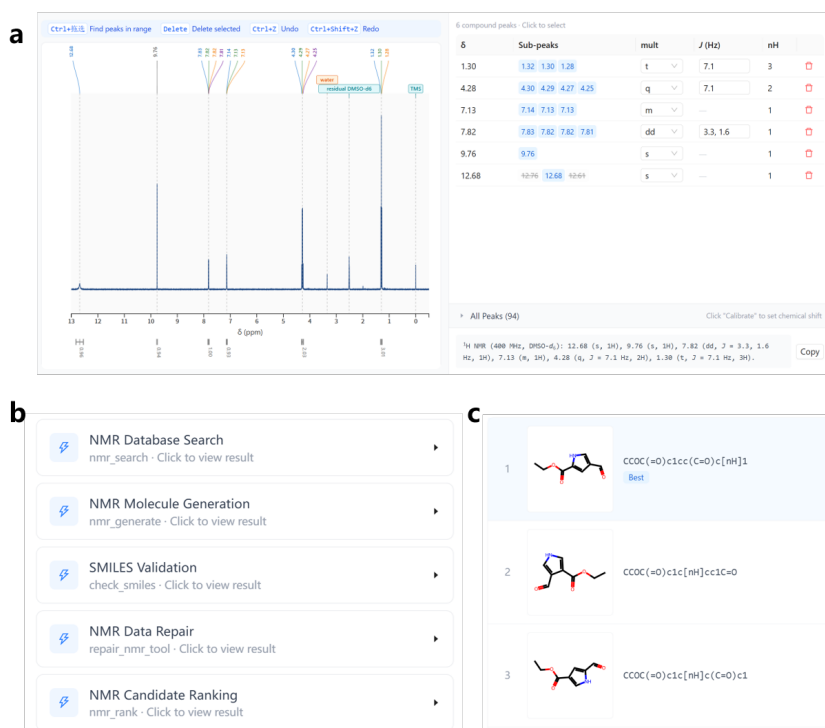


Figure 4: A comprehensive case study of elucidating molecular structure from FID data: (a) transformation of FID data into spectrum and multiplicity analysis; (b) agentic reasoning for structural elucidation; (c) reranking of candidate structures and final structure identification.

6.1 Stage I: Signal Processing and Feature Extraction

The process initiated with the acquisition of raw FID data from both ^1H and ^{13}C NMR experiments. SpecXMaster’s signal processing module directly performed automated Fourier transformation, phase correction, and baseline adjustment. The system successfully extracted quantitative multiplicity information, translating the complex spectral waves into a standardized textual format. For the ^1H and ^{13}C NMR spectrum, the extracted multiplicity text were as follows:

^1H NMR(400 MHz, $DMSO-d_6$): δ 12.69 (s, 1H), 9.77 (s, 1H), 7.82 (dd, $J = 3.4, 1.6$ Hz, 1H), 7.13 (dd, $J = 2.1, 1.8$ Hz, 1H), 4.23 (q, $J = 7.1$ Hz, 2H), 1.30 (t, $J = 7.0$ Hz, 3H). ^{13}C NMR(101 MHz, $DMSO-d_6$): δ 185.8, 160.1, 131.1, 126.7, 124.6, 113.1, 60.3, 14.2.

By converting the raw signals into this intermediate "Multiplicity Text," the framework effectively bridged the gap between physical data and chemical logic, ensuring that no critical coupling information was lost during preprocessing.

6.2 Stage II: Agentic Reasoning and Structural Elucidation

In the second stage, SpecXMaster performs structure elucidation through an agent-controlled tool-use process over the candidate space. Starting from the multiplicity text and molecular formula, the agent first uses **Generate** to propose an initial set of candidate structures. In this case, the correct molecule is not produced directly, but the generated candidates provide a reasonable starting point for subsequent exploration. The agent then invokes **Search** to expand the candidate pool with structurally related molecules from external databases. Although this step still does not return the exact target structure, it introduces candidates with a more plausible core scaffold, which provides a much stronger basis for downstream refinement. Next, the agent applies **Repair** to modify locally inconsistent structural fragments and correct scaffold-level details, gradually moving the candidate pool closer to the ground-truth molecule. Finally, **Rerank** is used to reorder the refined candidates according to spectrum–structure consistency, so that the correct structure can be prioritized at the top of the final list. This example illustrates the core advantage of the agentic framework: rather than relying on a single-step prediction, the agent progressively improves candidate quality through generate–search–repair–rerank interactions until the final structure is recovered. Other selected examples and their top-k reranked result are shown in **Appendix B**.

7 Future Outlook

7.1 Towards Multi-dimensional and Multi-modal Structural Elucidation

The future roadmap of SpecXMaster envisions a transition from an NMR-centric framework to a comprehensive multi-dimensional and multi-modal elucidation platform capable of addressing more complex chemical challenges. A primary focus will be the deep integration of 2D NMR spectroscopy, including HSQC, HMBC, COSY, and NOESY. By leveraging the high-order atomic connectivity and spatial proximity constraints provided by 2D spectra as inputs for the Agentic RL model, the system will significantly enhance its accuracy in identifying complex organic molecules, natural products, and subtle structural isomers. Furthermore, to meet the demands of real-world research, SpecXMaster will incorporate a specialized module for mixture analysis and quantitative yield determination. Through advanced spectral deconvolution techniques, the platform will not only achieve qualitative identification of multiple components but also perform quantitative NMR (qNMR) analysis to directly calculate product purity and reaction yields. By synergizing these capabilities with other modalities such as Infrared (IR) functional group features and Mass Spectrometry (LC-MS/GC-MS) fragmentation patterns, the system will emulate the holistic reasoning of human experts. This integration of reactant fragments and reaction context will allow the framework to perform cross-validation even in cases of signal overlap or missing data, establishing a closed-loop cognitive process from raw signals to precise structural determination.

7.2 Platform Ecosystem and UniLab OS Integration

The scalability and practical utility of SpecXMaster will be expanded through its integration into a broader, automated laboratory ecosystem. **Closed-Loop Autonomous Elucidation via UniLab OS:** To bridge the gap between digital decision-making and embodied experimentation, we will integrate SpecXMaster with UniLab OS, an AI-native operating system for autonomous laboratories [53]. Using UniLab's *Action/Resource/Action&Resource* (A/R/A&R) model and transactional protocols, the platform will enable for a seamless "dry-wet" closed loop. This integration facilitates direct instrument connection for end-to-end structural analysis, allowing agents to autonomously trigger re-acquisition or experimental validation to resolve structural discrepancies. **Collaborative Ecosystem and Customized Development:** SpecXMaster aims to foster a shared intelligent elucidation ecosystem by collaborating with leading academic research groups and industrial partners. This collaboration will drive the co-creation of standardized datasets and the advancement of domain-specific models. Additionally, we will provide customized model development tailored to proprietary customer datasets, offering bespoke solutions that address unique chemical spaces and specific industrial requirements.

8 Conclusion

In this work, we presented SpecXMaster, a novel intelligent framework that redefines the paradigm of NMR spectral interpretation through Agentic RL. By incorporating FID processing into an end-to-end pipeline, SpecXMaster overcomes the critical limitations of conventional expert-dependent methods, which are often hindered by human bias, variability, and the scarcity of specialized expertise. A key strength of our approach is the ability to interface directly with raw FID data rather than relying on simplified peak tables, ensuring that no critical spectral information is lost during the interpretation process. Through iterative reasoning and the integration of a multi-tool environment—including candidate generation, database search, and physics-guided local repair—SpecXMaster mimics the self-reflective logical deduction of professional spectroscopists. Experimental results demonstrate that SpecXMaster significantly outperforms existing one-shot models and general-purpose LLM, particularly in handling complex structural elucidation and "hard-case" candidates through hyperbolic representation learning. As a robust and scalable solution, SpecXMaster not only bridges the gap between raw physical signals and actionable molecular insights but also serves as a foundational component for the future of AI-driven, closed-loop scientific discovery in organic chemistry.

References

- [1] Abdul-Hamid Emwas, Kacper Szczepski, Benjamin Gabriel Poulson, Kousik Chandra, Ryan T McKay, Manel Dhahri, Fatimah Alahmari, Lukasz Jaremko, Joanna Izabela Lachowicz, and Mariusz Jaremko. Nmr as a "gold standard" method in drug design and discovery, 2020.
- [2] Gary Tom, Stefan P. Schmid, Sterling G. Baird, Yang Cao, Kouros Darvish, Han Hao, Stanley Lo, Sergio Pablo-García, Ella M. Rajaonson, Marta Skreta, Naruki Yoshikawa, Samantha Corapi, Gun Deniz Akkoc, Felix Strieth-Kalthoff, Martin Seifrid, and Alán Aspuru-Guzik. Self-driving laboratories for chemistry and materials science. *Chemical Reviews*, 124(16):9633–9732, Aug 2024.
- [3] Jarosław M. Granda, Liva Donina, Vincenza Dragone, De-Liang Long, and Leroy Cronin. Controlling an organic synthesis robot with machine learning to search for new reactivity. *Nature*, 559(7714):377–381, Jul 2018.
- [4] Susanta Das and Jr. Merz, Kenneth M. Exploring the frontiers of computational nmr: Methods, applications, and challenges. *Chemical Reviews*, 125(19):9256–9295, Sep 2025.
- [5] Kehan Guo, Yili Shen, Gisela Abigail Gonzalez-Montiel, Yue Huang, Yujun Zhou, Mihir Surve, Zhichun Guo, Prayel Das, Nitesh V Chawla, Olaf Wiest, and Xiangliang Zhang. Artificial intelligence in spectroscopy: Advancing chemistry from prediction to generation and beyond. 2025.
- [6] Fanjie Xu, Wentao Guo, Feng Wang, Lin Yao, Hongshuai Wang, Fujie Tang, Zhifeng Gao, Linfeng Zhang, Weinan E, Zhong-Qun Tian, et al. Toward a unified benchmark and framework for deep learning-based prediction of nuclear magnetic resonance chemical shifts. *Nature Computational Science*, 5(4):292–300, 2025.
- [7] Yongqi Jin, Yecheng Wang, Jun-jie Wang, Rong Zhu, Guolin Ke, et al. From human labels to literature: Semi-supervised learning of nmr chemical shifts at scale. *arXiv preprint arXiv:2601.18524*, 2026.
- [8] Frank Hu, Michael S Chen, Grant M Rotskoff, Matthew W Kanan, and Thomas E Markland. Accurate and efficient structure elucidation from routine one-dimensional nmr spectra using multitask machine learning. *ACS Central Science*, 10(11):2162–2170, 2024.
- [9] Yunyue Su, Jiahui Chen, Zao Jiang, Zhenyi Zhong, Liang Wang, and Qiang Liu. Language models can understand spectra: A multimodal model for molecular structure elucidation. *arXiv preprint arXiv:2508.08441*, 2025.
- [10] Shuaike Shen, Jiaqing Xie, Zhuo Yang, Antong Zhang, Shuzhou Sun, Ben Gao, Tianfan Fu, Biqing Qi, and Yuqiang Li. Molspectllm: A molecular foundation model bridging spectroscopy, molecule elucidation, and 3d structure generation. *arXiv preprint arXiv:2509.21861*, 2025.

- [11] Edwin Chacko, Rudra Sondhi, Arnav Praveen, Kylie L Luska, and Rodrigo Alejandro Vargas Hernandez. Spectro: A multi-modal approach for molecule elucidation using ir and nmr data. 2024.
- [12] Yongqi Jin, Jun-Jie Wang, Fanjie Xu, Xiaohong Ji, Zhifeng Gao, Linfeng Zhang, Guolin Ke, Rong Zhu, et al. NMR-Solver: Automated structure elucidation via large-scale spectral matching and physics-guided fragment optimization. *arXiv preprint arXiv:2509.00640*, 2025.
- [13] Sriram Devata, Bhuvanesh Sridharan, Sarvesh Mehta, Yashaswi Pathak, Siddhartha Laghuvapurapu, Girish Varma, and U Deva Priyakumar. Deepspinn—deep reinforcement learning for molecular structure prediction from infrared and 13 c nmr spectra. *Digital Discovery*, 3(4):818–829, 2024.
- [14] Jun-Jie Wang, Yongqi Jin, Chen-Yu Zhi, Yu-Jie Liu, Xu-Hao Huang, Fanjie Xu, Xiaohong Ji, Xi Fang, Haoyi Tao, Weinan E, Linfeng Zhang, Guolin Ke, and Rong Zhu. Nmrxp: A database of 3.3 million experimental nmr spectra. *Scientific Data*, 12(1), Dec 2025.
- [15] Jonathan J. Helmus and Christopher P. Jaroniec. Nmrglue: an open source Python package for the analysis of multidimensional NMR data. *Journal of Biomolecular NMR*, 55(4):355–367, 2013.
- [16] Richard R. Ernst, Geoffrey Bodenhausen, and Alexander Wokaun. *Principles of Nuclear Magnetic Resonance in One and Two Dimensions*. Oxford University Press, Oxford, 1987.
- [17] E. Bartholdi and R. R. Ernst. Fourier spectroscopy and the causality principle. *Journal of Magnetic Resonance*, 11(1):9–19, 1973.
- [18] James W. Cooley and John W. Tukey. An algorithm for the machine calculation of complex Fourier series. *Mathematics of Computation*, 19(90):297–301, 1965.
- [19] Li Chen, Zhiqiang Weng, LaiYoong Goh, and Marc Garland. An efficient algorithm for automatic phase correction of NMR spectra based on entropy minimization. *Journal of Magnetic Resonance*, 158(1–2):164–168, 2002.
- [20] Donald Erb. pybaselines: A Python library of algorithms for the baseline correction of experimental data.
- [21] Reto Koradi, Martin Billeter, Max Engeli, Peter Güntert, and Kurt Wüthrich. Automated peak picking and peak integration in macromolecular NMR spectra using AUTOPSY. *Journal of Magnetic Resonance*, 135(2):288–297, 1998.
- [22] Carlos Cobas. NMR signal processing, prediction, and structure verification with machine learning techniques. *Magnetic Resonance in Chemistry*, 58(6):512–519, 2020.
- [23] Eric Jonas and Stefan Kuhn. Rapid prediction of NMR spectral properties with quantified uncertainty. *Journal of Cheminformatics*, 11(1):50, 2019.
- [24] Mikhail Elyashberg and Dimitris Argyropoulos. Computer-assisted structure elucidation (CASE): Current and future perspectives. *Magnetic Resonance in Chemistry*, 59(7):669–690, 2021.
- [25] Alfarius Eko Nugroho and Hiroshi Morita. Computationally-assisted discovery and structure elucidation of natural products. *Journal of Natural Medicines*, 73(4):687–695, 2019.
- [26] Timo Schick, Jane Dwivedi-Yu, Roberto Dessi, Roberta Raileanu, Maria Lomeli, Eric Hambro, Luke Zettlemoyer, Nicola Cancedda, and Thomas Scialom. Toolformer: Language models can teach themselves to use tools. In *Advances in Neural Information Processing Systems (NeurIPS)*, 2023.
- [27] Ehud Karpas, Omri Abend, Yonatan Belinkov, Barak Lenz, Opher Lieber, Nir Ratner, Yoav Shoham, Hofit Bata, Yoav Levine, Kevin Leyton-Brown, Dor Muhlgay, Noam Rozen, Erez Schwartz, Gal Shachaf, Shai Shalev-Shwartz, Amnon Shashua, and Moshe Tenenholz. Mrkl systems: A modular, neuro-symbolic architecture that combines large language models, external knowledge sources and discrete reasoning. *arXiv preprint arXiv:2205.00445*, 2022.

- [28] Shunyu Yao, Jeffrey Zhao, Dian Yu, Nan Du, Izhak Shafran, Karthik Narasimhan, and Yuan Cao. React: Synergizing reasoning and acting in language models. In *International Conference on Learning Representations (ICLR)*, 2023.
- [29] Yongliang Shen, Kaitao Song, Xu Tan, Dongsheng Li, Weiming Lu, and Yueting Zhuang. Hugginggpt: Solving ai tasks with chatgpt and its friends in hugging face. In *Advances in Neural Information Processing Systems*, 2023.
- [30] Fanjie Xu, Jinyuan Hu, Jingxiang Zou, Junjie Wang, Boying Huang, Zhifeng Gao, Xiaohong Ji, Zhong-Qun Tian, Fujie Tang, Jun Cheng, et al. Synergistic cross-modal learning for experimental nmr-based structure elucidation. *arXiv preprint arXiv:2602.08752*, 2026.
- [31] Sunghwan Kim, Jie Chen, Tiejun Cheng, Asta Gindulyte, Jia He, Siqian He, Qingliang Li, Benjamin A Shoemaker, Paul A Thiessen, Bo Yu, et al. Pubchem 2025 update. *Nucleic acids research*, 53(D1):D1516–D1525, 2025.
- [32] Yu A Malkov and Dmitry A Yashunin. Efficient and robust approximate nearest neighbor search using hierarchical navigable small world graphs. *IEEE transactions on pattern analysis and machine intelligence*, 42(4):824–836, 2018.
- [33] Hannes H. Loeffler, Jiazhen He, Alessandro Tibo, Jon Paul Janet, Alexey Voronov, Lewis H. Mervin, and Ola Engkvist. Reinvent 4: Modern ai-driven generative molecule design. *Journal of Cheminformatics*, 16(1):20, 2024.
- [34] Zhenpeng Zhou, Steven Kearnes, Li Li, Richard N. Zare, and Patrick Riley. Optimization of molecules via deep reinforcement learning. *Scientific Reports*, 9(1):10752, 2019.
- [35] Samuel Gow, Viktor Kagi, Jovana Stamenkovic, Iryna Korshunova, Pedro Neves, and Pietro Lio. A review of reinforcement learning in chemistry. *Digital Discovery*, 1(5):551–573, 2022.
- [36] Jiazhen He, Alessandro Tibo, Jon Paul Janet, Eva Nittinger, Christian Tyrchan, Werngard Czechtizky, and Ola Engkvist. Evaluation of reinforcement learning in transformer-based molecular design. *Journal of Cheminformatics*, 16(1):95, 2024.
- [37] Martin Karplus. Contact electron-spin coupling of nuclear magnetic moments. *The Journal of chemical physics*, 30(1):11–15, 1959.
- [38] Maximilian Nickel and Douwe Kiela. Poincaré embeddings for learning hierarchical representations. In *Advances in Neural Information Processing Systems*, 2017.
- [39] Maximilian Nickel and Douwe Kiela. Learning continuous hierarchies in the lorentz model of hyperbolic geometry. In *Proceedings of the 35th International Conference on Machine Learning*, pages 3779–3788, 2018.
- [40] Octavian-Eugen Ganea, Gary Bécigneul, and Thomas Hofmann. Hyperbolic neural networks. In *Advances in Neural Information Processing Systems*, 2018.
- [41] Kelin Wu, Xin Hong, Wenyu Zhu, Bowen Gao, Wei-Ying Ma, and Yanyan Lan. Beyond lipschitz: Ranking binding affinity in hyperbolic space. *bioRxiv*, 2026.
- [42] Gengmo Zhou, Zhifeng Gao, Qiankun Ding, Hang Zheng, Hongteng Xu, Zhewei Wei, Linfeng Zhang, and Guolin Ke. Uni-mol: A universal 3d molecular representation learning framework. In *The eleventh international conference on learning representations*, 2023.
- [43] Mike Lewis, Yinhan Liu, Naman Goyal, Marjan Ghazvininejad, Abdelrahman Mohamed, Omer Levy, Veselin Stoyanov, and Luke Zettlemoyer. Bart: Denoising sequence-to-sequence pre-training for natural language generation, translation, and comprehension. In *Proceedings of the 58th annual meeting of the association for computational linguistics*, pages 7871–7880, 2020.
- [44] Richard S. Sutton and Andrew G. Barto. *Reinforcement Learning: An Introduction*. MIT Press, 2 edition, 2018.

- [45] Minghao Li, Yingxiu Zhao, Bowen Yu, Feifan Song, Hangyu Li, Haiyang Yu, Zhoujun Li, Fei Huang, and Yongbin Li. Api-bank: A comprehensive benchmark for tool-augmented llms. In *Proceedings of the 2023 Conference on Empirical Methods in Natural Language Processing*, pages 3102–3120, 2023.
- [46] Shishir G. Patil, Tianjun Zhang, Xin Wang, and Joseph E. Gonzalez. Gorilla: Large language model connected with massive apis. In *Advances in Neural Information Processing Systems*, 2024.
- [47] Zhihong Shao, Peiyi Wang, Qihao Zhu, Runxin Yang, Junxiao Xu, Miao Zheng, Ce Zhang, Ming Li, Y. Wu Gao, Yu Qiao, and Ping Luo. Deepseekmath: Pushing the limits of mathematical reasoning in open language models. *arXiv preprint arXiv:2402.03300*, 2024.
- [48] Guojiang Zhao, Zixiang Lu, Yutang Ge, Sihang Li, Zheng Cheng, Haitao Lin, Lirong Wu, Hanchen Xia, Hengxing Cai, Wentao Guo, Hongshuai Wang, Mingjun Xu, Siyu Zhu, Guolin Ke, Linfeng Zhang, and Zhifeng Gao. Molreasoner: Toward effective and interpretable reasoning for molecular llms. *arXiv preprint arXiv:2508.02066*, 2025.
- [49] Zhiwei Li, Yong Hu, and Wenqing Wang. Encouraging good processes without the need for good answers: Reinforcement learning for llm agent planning. *arXiv preprint arXiv:2508.19598*, 2025.
- [50] OpenAI. Introducing gpt-5.2. <https://openai.com/index/introducing-gpt-5-2/>, 2025. Accessed: 2026-03-17.
- [51] An Yang, Baosong Yang, Beichen Zhang, Binyuan Hui, Bo Zheng, Bowen Yu, Chengyuan Li, Dayiheng Huang, Fei Li, Haoran Liu, et al. Qwen2.5 technical report. *arXiv preprint arXiv:2412.15115*, 2024.
- [52] Long Ouyang, Jeff Wu, Xu Jiang, Diogo Almeida, Carroll L. Wainwright, Pamela Mishkin, Chong Zhang, Sandhini Agarwal, Katarina Slama, Alex Ray, John Schulman, Jacob Hilton, Fraser Kelton, Luke Miller, Maddie Simens, Amanda Askell, Peter Welinder, Paul Christiano, Jan Leike, and Ryan Lowe. Training language models to follow instructions with human feedback. *Advances in Neural Information Processing Systems*, 2022.
- [53] Jing Gao, Junhan Chang, Haohui Que, Yanfei Xiong, Shixiang Zhang, Xianwei Qi, Zhen Liu, Jun-Jie Wang, Qianjun Ding, Xinyu Li, Ziwei Pan, Qiming Xie, Zhuang Yan, Junchi Yan, and Linfeng Zhang. Unilabos: An ai-native operating system for autonomous laboratories. 2025.

A Authorship and Acknowledgments

Please cite this work as “DP Technology (2026)”.

Correspondence regarding this technical report can be sent to jixh@dp.tech, gaozf@dp.tech

Core Contributor

Yutang Ge
Yaning Cui
Hanzheng Li
Jun-Jie Wang

Project Lead

Xiaohong Ji
Zhifeng Gao

Contributors

Fanjie Xu
Jinhan Dong
Yongqi Jin
DongXu Cui
Peng Jin
Guojiang Zhao
Hengxing Cai
Tianci Yangfeng

Team Management

Rong Zhu
Linfeng Zhang

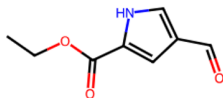
B Selected Examples of Internal Case Study

Based on feedback from Professor Rong Zhu’s group during SpecXMaster’s internal testing, the table below presents the top-k ranking of candidate SMILES paired with their real structures, generated from inputs of multiplicity text and molecular formula

SMILES	Top-k
<chem>C/C(C1=CC=CC=C1)=C\CC(OC2=CC=C(C(OC)=O)C=C2)C3=CC=CC=C3</chem>	1
<chem>Cl[C@H]1CCCC2=CC=CC=C21</chem>	1
<chem>O=C(/C(C/C(C1=CC=CC=C1)=O)=C/NC2=CC=CC=C2)=C\NC3=CC=CC=C3)C4=CC=CC=C4</chem>	1
<chem>OC(C=C1C)=CC(C)=C1C2=NC(C3=CC=CC(C4=C(C)C=C(O)C=C4C)=N3)=CC=C2</chem>	1
<chem>O=C(OC(C)(C)N)CCCC(Cl)C1</chem>	1
<chem>O=C(C1=C(N)SC(C2=CC=C3C=CC=CC3=C2)C1)OCC</chem>	1
<chem>O=C1N(CC(C)=O)C(C2=CC=CC=C21)=O</chem>	1
<chem>CC(C)(O)C1=CC=C(C#N)C=C1</chem>	1
<chem>C=C=C1CC(C(=O)OCc2ccccc2)=C(OCc2ccccc2)O1</chem>	1
<chem>O=c1[nH]c(-c2ccccc2)co1</chem>	1
<chem>COc1ccccc1CN1CCN(Cc2ccccc2OC)C1</chem>	1
<chem>CC(=CC1CN(Cc2ccccc2)CCN1Cc1ccccc1)c1ccccc1</chem>	1
<chem>C#CC1(c2ccccc(Cl)c2)COC(N)=C1C#N</chem>	1
<chem>O=C(C(C=CC=C1)=C1C2=O)N2OCC3=CSC=N3</chem>	1
<chem>C#CC1=CN(S(C2=CC=C(C)C=C2)(=O)=O)C3=C1C=CC(Br)=C3</chem>	1
<chem>CC(=O)Nc1cccc(C=O)c1</chem>	1
<chem>OC(C1C(C(OC)=O)=C(C(OC)=O)C2(O1)C3=CC=CC=C3)=C2C4)CN4S(C5=CC=C(C)C=C5)(=O)=O</chem>	2
<chem>O=C(C1=CC=CS1)OCCC/C=C/CCCOC(C2=CC=CS2)=O</chem>	3
<chem>CC1(C)CC=C(OS(=O)(C(F)(F)F)=O)C([Si](C)(C)C)=C1</chem>	4
<chem>F/C(N1C(C=C(C)C(C)=C2)=C2N=N1)=C\C3=CC=C(C(OC)=O)C=C3</chem>	4

C Detailed Structure Elucidation Report

1. Most Likely Molecular Structure



2. Identification Logic and Data Matching

Molecular Formula Verification: This molecular structure is ethyl 4-formyl-1H-pyrrole-2-carboxylate. Its molecular formula is $C_8H_9NO_3$, with a calculated degree of unsaturation (Ω) of 5 (pyrrole ring 2 + carbonyl groups 2 + ester group 1), which is fully consistent with the molecular formula.

¹H NMR Analysis:

- δ 12.68 (s, 1H): Located at an extremely downfield position, this corresponds to the NH proton on the pyrrole ring. Due to the electronegativity of the nitrogen atom and ring current effects, and its tendency to form hydrogen bonds in DMSO-d₆, the signal appears as a broad singlet.
- δ 9.76 (s, 1H): A characteristic aldehyde hydrogen (-CHO) signal, appearing as a singlet at an extremely downfield position.
- δ 7.82 (dd, $J = 3.3, 1.6$ Hz, 1H): Assigned to the hydrogen at the C5 position of the pyrrole ring. The downfield position is due to the electron-withdrawing inductive effect of the adjacent aldehyde group and ring current effects; the splitting pattern results from long-range coupling with the C3 hydrogen and NH.
- δ 7.13 (m, 1H): Assigned to the hydrogen at the C3 position of the pyrrole ring. Located in the aromatic region, it is shifted slightly upfield relative to the C5 hydrogen due to the influence of the ester group.
- δ 4.28 (q, $J = 7.1$ Hz, 2H): The methylene group (-CH₂-) of the ester, shifted downfield by the strong electron-withdrawing effect of the oxygen atom, and split into a quartet by coupling with the adjacent methyl group.
- δ 1.30 (t, $J = 7.1$ Hz, 3H): The terminal methyl group (-CH₃) of the ester, located at high field, split into a triplet by coupling with the methylene group.

¹³C NMR Analysis:

- δ 186.3: Assigned to the aldehyde carbonyl carbon (-CHO), located at a characteristically extreme downfield position.
- δ 160.6: Assigned to the ester carbonyl carbon (-COO-).
- δ 131.5, 127.2, 125.1, 113.6: These four signals correspond to the four carbon atoms on the pyrrole ring. Among them, δ 131.5 and 127.2 typically correspond to substituted carbons bearing electron-withdrawing groups (aldehyde and ester) or adjacent carbons strongly influenced by them.
- δ 60.8: Assigned to the oxygen-bonded methylene carbon (-OCH₂-).
- δ 14.7: Assigned to the methyl carbon of the ethyl group (-CH₃), located at the highest field position.

Key NMR Signatures: The most distinctive feature of this structure is the two prominent downfield singlets (δ 12.68 and 9.76), which unambiguously identify the presence of an active hydrogen (NH) and an aldehyde group. In the ¹³C NMR, δ 186.3 and 160.6 clearly distinguish the aldehyde from the ester carbonyl. The main basis for excluding other isomers (such as 2,3- or 2,5-substituted) is the chemical shift difference between the two ring hydrogens and their small coupling constants (J values), which are consistent with a 2,4-disubstituted pyrrole, where the two ring protons are in non-adjacent positions.